29th Congress of the International Council of the Aeronautical Sciences
St. Petersburg, Russia; September 7-12, 2014

NUMERICAL SIMULATION OF UNSTEADY FLOWS AROUND HIGH-LIFT CONFIGURATIONS

S.Bosnyakov*, I.Kursakov*, A.Lysenkov*, S.Mikhaylov*
***Central Aerohydrodynamic Institute (TsAGI)**
Zhukovsky street, 1, 140185 Zhukovsky, Moscow Region, Russian Federation

Keywords: *cryogenics, digital approach to wind tunnel, high-lift wing, CFD zonal approach*

Abstract

The work presented has been performed in the frame of the DESIREH project (FP7) funded by the EC. This project contributes to the realization of the ACARE Vision 2020 for significantly greener aircraft and a reduced time to market by improving the aerodynamics of the High-Lift system. This should be achieved by considering - at the same time and in coordinated approach - the numerical design methodology and the measurement techniques for cryogenic conditions for an advanced laminar wing design. The final aerodynamic tests of the high-lift aircraft model were performed in ETW. The main goal of the TsAGI team was to estimate the effects of wind-tunnel walls on the model characteristics.

1 Introduction

One of the key problems formulated in "Horizon 2020" program is the creation of a "green" aircraft on the base of the best innovations of present day aerodynamics. A solution of the above problem is possible using powerful computers and CFD technologies. TsAGI has vast experience in the development and implementation of complex methods. Some results are published in [1,2], where "Electronic wind tunnel" was described. This code is used in TsAGI since 1996. It permits to solve the stationary (RANS) and non-stationary (URANS) Navier-Stokes equations with Reynolds-averaging. A possibility to simulate large-scale vortices (LES) is realized. Special boundary conditions, such as "wind tunnel start", "permeable walls" (perforated and slotted), "runway simulator" and "plenum chamber walls" are discussed in details. It is mentioned that the code effectively uses chimera-type grids based on the original "connect" technology. Practical aspects are developed. Many grid templates with special blocks for model and wind tunnel parts are prepared in advance. It permits to change model in "Electronic Wind Tunnel" operatively. An important algorithm for grid rebuilding, in the case of changing the model incidence and slip angles, has also been developed and is working reliably. Initially (1996), the code was tailored for the configuration of the T-128 wind tunnel of TsAGI. Later on (2006), the version for the cryogenic European Transonic Wintunnel (ETW) has been created. More recently, a specific code has been developed in 2008 for the TsAGI T-104 wind tunnel (takeoff/landing regimes) with a "runway simulation" and an open test section.

It is not subject for arguing that wind tunnel tests are almost the only source of high-end reliable data prior to a flight test campaign. So, experimental results are included in this article as an essential part of the theoretical and CFD study. Among others, the authors have chosen results from ETW obtained at flight Re numbers with low dynamic pressure. It creates new requirements to numerical methods and forces taking into account cryogenic phenomena and multidisciplinary approaches. All relevant problems are simultaneously present when a complex task e.g. as high lift system is under investigation. The structure of the flow with deployed slats and flaps is extremely intricate due to the interaction of numerous phenomena. The flow shows typical viscous behavior with

turbulent boundary layers forming the flow structure. In spite of low Mach numbers ($M \sim 0.2$), corresponding to landing regimes, deflected slats may create supersonic zones and separation bubbles. Nevertheless, at moderate incidence angles the averaged flow may be successfully calculated using available RANS methods. It can't give answers to all questions as, for example, the prediction of the drag coefficient is still a big problem up to now. But real problems appear at high incidences when non-stationary separation zones and wakes will make the task unbelievably complicated. From the one hand, this approach is using explicit numerical schemes for unsteady phenomena modeling. From the other hand, multiscale features create CFL problems which are impossible to be solved without implicit approaches. It is a well-known fact that the time scale for different physical processes may differ essentially (from 10 to 100 times). As a result, a huge number of calculations is the logical result for explicit based methods applied for such cases. Contrary to this, implicit methods for multiscale situations show good "economics" but low quality of results. A possible solution for the described problem is to use zonal approaches, which include implicit numerical schemes for tiny scale physical phenomena (inner part of the boundary layer) and explicit ones for the remaining part of the computational area. Such an approach simultaneously provides a high level of resolution and an acceptable computing time.

Currently, the scientific development of approaches by the application of the Reynolds averaged Navier-Stokes (RANS, URANS) system of equations has been completed. This, however, does not mean that relevant work has entirely been stopped. At the same time, the major efforts of researchers are directed to developing the LES (DES) methods [3]. Indeed, the internationally published differential models of turbulence [4] are, as a rule, tuned to the solution of a narrow class of problems and their implementation is justified only within the zonal approach. For example the known model [5] yields acceptable results in the near-wall regions with the developed turbulence boundary layer. Another popular model of turbulence, [6−8], in contrast, describes free turbulence much better than wall turbulence. A successful solution is the combined approach, for example, SST [9], in which a smooth transition from one model of turbulence to another depends on the function of remoteness from hard walls. A special topic in such calculations is the location of the region of laminar to turbulence transition. A new SST model with additional equations has been proposed allowing in a number of cases the solution of the defined problem [10].

To speed-up the calculations in the inviscid core, a method of fractional time stepping is proposed [1]. The idea of fractional time stepping is that the calculation in each cell is performed with the time step at the maximal possible Courant number. This leads to the numbers of interim time steps being different in different cells and they are selected that all the cells achieve the same layer of physical time at the some moment. All the calculations were performed on the basis of a full 3D non-stationary Reynolds equation system closed by the Menter SST turbulence model [9]. The basic variant of solver, which had been previously developed by the authors, is realized on the basis of a solution of a finite-volume numerical method of this equation system that has the second approximation order in all variables and includes the monotonic Godunov-Kolgan-Rodionov scheme for the approximation of convective fluxes, central-difference approximation of diffusive fluxes and a two-layer point-implicit approximation of source terms. A detailed description of such a method is given in [2]. The calculations are performed on a multiblock structured grid with hexahedral cells. This grid allows an irregular connection of blocks with a discontinuity of the grid lines at the block boundaries.

Appropriate experimental investigations have been performed in the European Transonic Windtunnel (ETW) by a consortium created in the frame of DeSiReH FP7 project under the leadership of J. Quest. This facility operates under cryogenic conditions. It permits to obtain flight Re numbers by means of pure nitrogen gas cooled down to cryogenic temperatures. Nevertheless the equilibrium state of gas is strictly watched to avoid condensation. On the

other hand, the simultaneously required increase in tunnel pressure by up to 4.5 bar affects density and, hence, intermolecular connections might play an essential role. As a result, the well-known gas state equation $p = \rho RT$ would not be valid anymore for such cases. At very low temperature the heat energy for an individual molecule is close to an energy step between levels and the quantum feature of the energy state is to be taken into account. As a consequence, the heat capacity is not constant and depending on temperature and density. The molecular viscosity cannot be approximated by the Sutherland law anymore, but, in fact, a more complicated function of temperature and density. Presently, the used empirical formula provides an accuracy of ~0.1% for the temperature interval $T = 65 \div 1073$ K and pressure levels up to 10^8Pa. The only chance to operate under such severe conditions is to use pure nitrogen [11]. This is realized in ETW.

It is known that codes with implemented 3D approaches work at the limits of available computers capacities. It results in a fact that computer methodology, as a rule, is closely adjusted to the capacity of computer system for maximal optimization of its resources. A major improvement is nowadays given by modern clusters with hundreds and thousands of processors. An essential factor is the exponential reduction of cost for such systems. It permits to include computational investigations into a technological cycle of experiment. In this article authors calculate not only the model but additionally the test-section of ETW with closed walls. Special attention is paid to the problem of turbulence level modeling at the entrance to the wind tunnel test section. It is clear that the complexity of the task is increasing numerously and essential extra time is required e.g. for building additional grids. Additional computer resources are used to calculate the flow field in the regions upstream and downstream of the model. The plenum chamber completes as an essential part the computer model. Otherwise, this approach gives already a chance to predict phenomena to be investigated prior to the preparation of the experiment itself.

2 Equations and Nnumerical Method

The flow in the vicinity of a high-lift wing features a rather complicated structure and an interaction of many physical effects. In spite of the low Mach numbers ($M \sim 0.2$) being considered here, which correspond to takeoff and landing regimes, there is high possibility of high-speed zones in the flow around the highly deflected slat. In the case of medium incidence angles, the time-averaged flow is stationary and can be simulated numerically with the use of RANS. Some problems regarding the correct prediction of the drag and lift coefficient of the wing are evident but more serious troubles arise in the case of large incidence angles, when, due to stall, there are non-stationary processes due to the interaction of developed separation zones with non-stationary vortex sheets downstream of the wing. The time-dependent Reynolds equation system closed by Menter [10] turbulence model is written as:

$$\frac{\partial \vec{u}}{\partial t} + \frac{\partial \vec{F}(\vec{u})}{\partial x} + \frac{\partial \vec{G}(\vec{u})}{\partial x} + \frac{\partial \vec{H}(\vec{u})}{\partial x} = \vec{W},$$

where

$$\vec{u} = \begin{bmatrix} \rho \\ \rho u \\ \rho v \\ \rho w \\ \rho E \\ \rho k \\ \rho \omega \end{bmatrix}, \quad \vec{W} = \begin{bmatrix} 0 \\ 0 \\ 0 \\ 0 \\ 0 \\ S(k) \\ S(\omega) \end{bmatrix},$$

$$\vec{F} = \begin{bmatrix} \rho V_n \\ \rho V_n u + p s_x + I_{xn} \\ \rho V_n v + p s_y + I_{yn} \\ \rho V_n w + p s_z + I_{zn} \\ V_n \cdot (\rho E + p) + \left(I_{xn} u + I_{yn} v + I_{zn} w\right) + (q_n + \rho \sigma_n) \\ \rho V_n k + T_n^k \\ \rho V_n \omega + T_n^\omega \end{bmatrix}$$

$V_n = u s_x + v s_y + w s_z$ - normal to border velocity,

$\tau_{in} = \tau_{ix} s_x + \tau_{iy} s_y + \tau_{iz} s_z$ - viscous tangential tense,

$\rho R_{in} = \rho R_{ix} s_x + \rho R_{iy} s_y + \rho R_{iz} s_z$ - turbulent tangential tense,

$I_{in} = \tau_{in} + \rho R_{in}$ - total tangential tense,

$T_n^k = T_x^k s_x + T_y^k s_y + T_z^k s_z$ - total diffusive turbulent kinetic energy *k* flux,

$T_n^\omega = T_x^\omega s_x + T_y^\omega s_y + T_z^\omega s_z$ - total diffusive frequency ω flux,

$$T_x^k = -\left(\mu_{lam} + \frac{\mu_T}{\mathrm{Pr}_{turb}^k}\right)\cdot\frac{\partial k}{\partial x},$$

$$T_x^\omega = -\left(\mu_{lam} + \frac{\mu_T}{\mathrm{Pr}_{turb}^\omega}\right)\cdot\frac{\partial \omega}{\partial x}.$$

Turbulent viscosity is $\mu_T = \rho\frac{k}{\omega}\cdot F_{wall}$, where

$$F_{wall} = \frac{1}{\max\left\{\frac{1}{\alpha^*}; \frac{\Omega\cdot F_2}{a_1\cdot\omega}\right\}},$$

$$\alpha^* = \begin{cases} \dfrac{0.144 + \mathrm{Re}_T}{6 + \mathrm{Re}_T}, & \mathrm{SST(ver.1)}, \\ 1, & \mathrm{SST(ver.2)}, \end{cases}$$

$$\Omega = \begin{cases} \sqrt{\Omega_{\mathrm{ver1}}}, & \mathrm{SST(ver.1)}, \\ \sqrt{\Omega_{\mathrm{ver1}}}, & \mathrm{SST(ver.2)}, \end{cases}$$

$$\Omega_{\mathrm{ver1}} = \left(\frac{\partial u}{\partial y} - \frac{\partial v}{\partial x}\right)^2 + \left(\frac{\partial u}{\partial z} - \frac{\partial w}{\partial x}\right)^2 + \left(\frac{\partial v}{\partial z} - \frac{\partial w}{\partial y}\right)^2,$$

$$\Omega_{\mathrm{ver2}} = 2\left[\left(\frac{\partial u}{\partial x}\right)^2 + \left(\frac{\partial v}{\partial y}\right)^2 + \left(\frac{\partial w}{\partial z}\right)^2\right] + \left(\frac{\partial u}{\partial y} + \frac{\partial v}{\partial x}\right)^2 + \left(\frac{\partial u}{\partial z} + \frac{\partial w}{\partial x}\right)^2 + \left(\frac{\partial v}{\partial z} + \frac{\partial w}{\partial y}\right)^2,$$

$$F_2 = \mathrm{th}\left(\mathrm{arg}_2^2\right), \quad \mathrm{arg}_2 = \max\left\{\frac{2\sqrt{k}}{\beta^*\omega y_w}; \frac{500\mu_{lam}}{\rho\omega y_w^2}\right\}.$$

Source terms look like:

$$S(k) = \left[\tilde{A}_k\frac{1}{\rho\omega} + \tilde{B}_k + \tilde{C}_k\rho\omega\right]\cdot\rho k,$$

$$S(\omega) = \tilde{D}_\omega\frac{1}{\rho\omega} + \tilde{A}_\omega + \tilde{B}_\omega\rho\omega + \tilde{C}_\omega(\rho\omega)^2,$$

$$\tilde{A}_k = S\cdot F_{wall}F_P\cdot\rho, \quad \tilde{B}_k = 0, \quad \tilde{C}_k = -\frac{\beta^*(1+F_c)}{\rho},$$

$$\tilde{D}_\omega = 2(1-F_1)\mathrm{Pr}_{turb2}^\omega\cdot\left[\frac{\partial k}{\partial x}\frac{\partial \omega}{\partial x} + \frac{\partial k}{\partial y}\frac{\partial \omega}{\partial y} + \frac{\partial k}{\partial z}\frac{\partial \omega}{\partial z}\right]\cdot\rho^2.$$

The explicit scheme is the best choice for non-stationary applications, when the time scale is comparable with the ratio between space scale and maximal eigenvalue, i.e. when $CFL \sim 1$. For such applications, the Runge-Kutta scheme is very popular but in the case of problems with large and medium time scales and with strong discrepancy of cell sizes, the restriction due to stability can be essentially less than the typical physical time of flow changes. This case is symptomatical, for example, in the presence of stall. Near-wall cells prescribe an extra-small time integration step. As a result, one needs integrations with huge values of the CFL number. It's well-known fact that calculation with $CFL >> 100$ can generally be performed without an accuracy alleviation. The better approach is seen by implementing another strategy to achieve appropriate quality combined with a good computational efficiency. This idea is based on inevitable choice of introducing a thin near-wall zone for applying an implicit scheme with dual-time stepping. In the outer part of flow, the calculation should be performed with $CFL < 1$ which gives high-quality description for the non-stationary processes. It is assumed to use the explicit scheme in this part of the flow. Such an approach permits to keep the high quality of the non-stationary process description and may be named as *Zonal Decomposition approach.*

Bellow, for simplicity, the schemes will be formulated for a scalar model equation that contains convective fluxes only.

$$\frac{\partial u}{\partial t} + \frac{\partial F(u)}{\partial x} = 0.$$

To speed up calculations of steady flows, the implicit scheme with global time stepping is used. This scheme may be represented by the following form:

$$\frac{u_i^{n+1}-u_i^n}{\tau}+ \\ +\frac{A_{i+1/2}\cdot\left[\tilde{U}_{i+1/2}^{n+1}-\tilde{U}_{i+1/2}^{n}\right]-A_{i-1/2}\cdot\left[\tilde{U}_{i-1/2}^{n+1}-\tilde{U}_{i-1/2}^{n}\right]}{h}+ \\ +\frac{F_{i+1/2}(u^n)-F_{i-1/2}(u^n)}{h}=0$$

In this example, both the approximation of the physical time derivative $\partial u/\partial t$ and the implicit part of the spatial operator has only the first accuracy order. Jacoby matrices $A_{i+1/2}=A(u_i^n,u_{i+1}^n)$ are calculated at the known time layer n. Only the explicit part of spatial operator is approximated using the 2nd accuracy order scheme. The system of algebraic linear equations is approximately solved by 6 iterations of the Gauss–Seidel method for block-diagonal matrices. At the beginning of the computation, the value of the global time step τ is not very large but it is increased gradually, tending to the given value of $CFL_{\max}$. If some problems concerning stability will arise, the time step is diminished temporarily; when the stability returns, the step begins to grow again. It is obvious that such an approach excludes any possibility of a correct simulation of any non-stationary phenomena. If the local value of the Courant number $CFL>>1$, one can't even speak about the approximation of the derivative $\partial u/\partial t$: the errors of approximation may be higher than the approximated derivative itself. The spatial operator is not approximated either because of the linearization of non–linear fluxes. Incomplete Gauss–Seidel iterations crown this list of errors. Otherwise, each global time step is performed very quickly (only several times slower than a single global time step with explicit scheme), and the scheme is generally stable; if the stationary solution is achieved, it provides the required 2nd accuracy order in space, because the stationary limit of equation above coincides with the stationary limit for the explicit scheme. If the stationary solution exists, the convergence to this stationary solution is usually better and essentially quicker than the convergence for explicit scheme with local–time stepping or with multigrid acceleration. So, this scheme is a very good choice for any stationary task solution but within the current work, the unsteady phenomena are subjects of interest. A dual-time stepping method is usually used for realization of the time-accurate implicit scheme instead of traditional methods for solving the large non-linear algebraic equation systems. The 2th order scheme in time is used and a fictitious non-stationary term is added:

$$\frac{\partial u}{\partial \xi}+\left(1+\frac{\tau_n}{\tau_{n-1}+\tau_n}\right)\frac{u-u_i^n}{\tau_n}-\frac{\tau_n}{\tau_{n-1}+\tau_n}\frac{u_i^n-u_i^{n-1}}{\tau_{n-1}}+ \\ +\frac{F_{i+1/2}(u)-F_{i-1/2}(u)}{h_i}=0.$$

Here, ξ refers to the pseudo-time. The stationary solution of the problem, when it is single, coincides with the solution of the discrete equation without a pseudo-time term: in the stationary limit $u=u^{n+1}$. Because it is time-marching method and we are interested in a stationary solution only, different methods of convergence acceleration may be used to obtain this solution. The high-efficient implicit scheme with strongly simplified implicit operator is implemented here:

$$\begin{cases} u_i^{(0)}=u_i^n, \\ \frac{u_i^{(k+1)}-u_i^{(k)}}{\Delta\xi}+\frac{3}{2}\frac{u_i^{(k+1)}-u_i^n}{\tau}-\frac{1}{2}\frac{u_i^n-u_i^{n-1}}{\tau}+ \\ +\frac{A_{i+1/2}\cdot\left[\tilde{U}_{i+1/2}^{(k+1)}-\tilde{U}_{i+1/2}^{(k)}\right]-A_{i-1/2}\cdot\left[\tilde{U}_{i-1/2}^{(k+1)}-\tilde{U}_{i-1/2}^{(k)}\right]}{h}+ \\ +\frac{F_{i+1/2}(u^{(k)})-F_{i-1/2}(u^{(k)})}{h}=0,\quad k=1,\ldots,M, \\ u_i^{n+1}=u_i^{(M)}. \end{cases}$$

Such a scheme has only the first order in pseudo-time that results both in the acceleration and in the stability. To speed-up calculations in the main part of the flow (out of near wall area), a *method of fractional time* stepping is used. The idea of fractional time stepping is that the calculation in each cell is performed with the

maximum possible time step but the numbers of *interim time steps* are different in different cells and they are chosen so as all the cells achieve the same layer of physical time at the same moment. When the same time layer is achieved, let's name it as a completion of *global time step*. For example, if an *interim* time step in the cell (A) is equal to $\tau_{\max}$, in (B) - $\tau_{\max}/2$ and in (C) - $\tau_{\max}/8$, then, during one *global* time step, one should perform one *interim* time step in the cell (A), two *interim* time steps in the cell (B) and eight *interim* time steps in the cell (C). Therefore, the *global* time step in each cell is divided (*fragmented*) into smaller *interim* time steps so as the *interim* time steps satisfy to the local CFL condition. That's why the procedure is named as *fractional time stepping*. This procedure reduces the total calculation time *in rational programming* and guaranties that the local value of stability coefficient ($C_{stab} \in [0.5;1]$) is used in each cell. The fractional time stepping is very easy to be implemented. That's why we preferred to go this way.

3 Model and Wind Tunnel Tests

The model under consideration consists of the fuselage and the high-lift wing supplied in DeSiReH with deflected Krueger slat and deflected flaps. It is attached to the wind tunnel ceiling by a peniche, see Fig. 1.

Fig. 1. Model in ETW. (Thanks to J. Quest and DeSiReH consortium)

Special features of ETW test capabilities are described in details in [12-13]. It is shown that Re number for half-models may be up to ~90 million (half wing 1.3 m). Main performances of this wind tunnel are listed below:

- Mach number range - 0.13÷1.35
- Test section size - 2×2.4×9 m
- Pressure range - 115÷450 kPa
- Temperature range - 110÷313K
- Capacity - 50 MW

The wind tunnel is using pure nitrogen as test gas. One of the main advantages of ETW is operating down to cryogenic conditions with the capability for controlling the dynamic pressure. This permits to avoid nonphysical airplane model deformation. To operate with low wall interference the test section being surrounded by a plenum chamber can be equipped with slots (in top, bottom and side-walls). The side walls are settled with 4 slots. The established porosity of one wall is *7.4%*. When a half model is tested at higher speeds, the slots may be opened to provide a total porosity of *4.6%*. The ETW operating system permits to support a high operating point stability, for example, for the Mach number, it is inside $\pm M=0.001$, total pressure fluctuations are lower than $\Delta P_0/P_0 \leq 0.002$ and total temperature fluctuations are restricted to $\pm 0.5K$.

The high lift half-model DLRF13-DS21 has been tested in the frame of the DeSiReH FP7 EU project by the ETW team. It had a scale 1:11.75 and the main wing was supplied with a Krueger slat at the leading edge and single-slot flaps at the trailing edge. Two configurations were under investigation: 1) reference; 2) optimized. There have been three present day measurement techniques simultaneously applied: Transition detection by Temperature Sensitive Paint (TSP), flow filed measurements by PIV and model deformations assessment by operating the Stereo Pattern Tracking system (SPT). Standard pressure distributions, moments and forces on the model were also measured according to industrially required quality. Tests were performed at $M=0.2$, $T_0=115K$, $P_0=335.6$ *kPa*, $Re=1.5–16.7$ million over an incidence range of $\alpha=-10^0 – 25^0$.

4 Mathematical Model and Grids

The copyright statement is included in the template and must appear in your final pdf document in the position, style and font size shown below.

The model geometry is provided by the partners of TsAGI in the DeSiReH project. The configuration consists of the high-lift wing and a fuselage. The wing of the model is supplied with deflected Krueger slat and deflected flap, as to be seen in Fig. 2. The deflection angles of the leading and trailing edges correspond to a landing setting. The lower wing surface contains a cut-out to store the moveable leading edge devices during cruise flight. The geometrical description corresponds to the wind tunnel model, which has been tested in ETW.

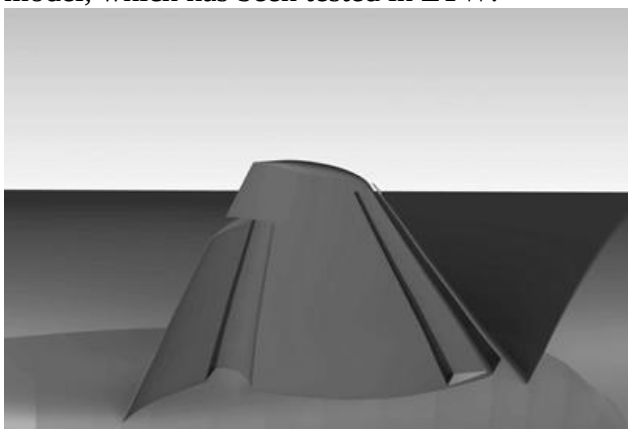

Fig. 2. Wing with deflected slat and flap

This model is presented inside the numerically generated ETW test section as to be seen in Fig. 3. The centre of model rotation corresponds to the real ETW one. Two wind tunnel configurations are considered. The first corresponds to the test section with closed slots, the second - to the one with open longitudinal slots. The starboard-side of the model is mounted to the tunnel ceiling attached to a peniche (Fig. 1). The incidence angle of the test article is changed by rotating the model on the peniche inside the test section. The important simplification introduced in the mathematical model of ETW is the separation of the common plenum chamber in two parts. This was done to reduce the number of cells of the computational grid. The following set of parameters and reference values was used: wing area S=0.45 m^2, mean aerodynamic chord MAC = 0.3 m. All dimensions correspond to the wind tunnel situation. The origin of the coordinate axis system is depicted at the left lower corner at the inlet of the ETW test section. The X-axis is directed downstream, the Y-axis is located in the symmetry plane in upper direction, the Z-axis is oriented from the left to the right wall. The point of model rotation has the coordinates x=3.677 m, y=2 m, z=1.2 m and is located at the upper wall. The nose of the model at zero incidence is located at x=2.241 m, y=1.9556 m, z=1.2154 m. The peniche thickness amounts to 0.0444 m. The divergence of the lower wind tunnel wall equals 0.55° with open slots and is 0.35° with closed slots.

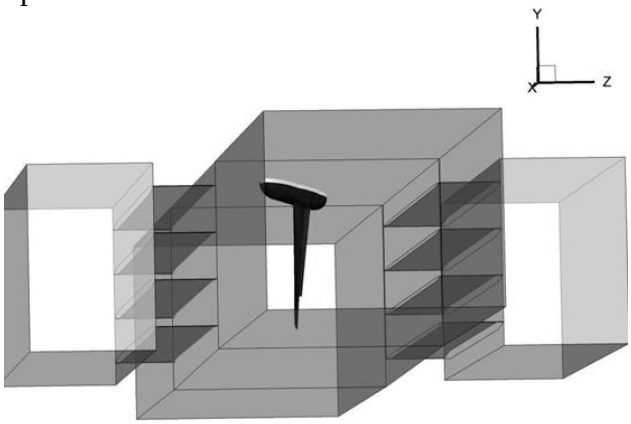

Fig. 3. Numerical Model of ETW including test-section with open slots and plenum chamber(s) as well as the model mounted on the peniche

A multi-block structured grid has been used for the task solution. The grid topology was adjusted in the way that allows the minimization of efforts needed for grid rebuilding due to a change of the angle of attack. The computational domain was divided in three independent parts:

- Central region including the fuselage and high-lift wing;
- Outer region including the model nose and the rear parts of the fuselage, peniche and WT ceiling;
- The outer region of the ETW test section.

The benefit of this generalization is the reusability of the unmodified grids of the parts 1 and 3 for variations of the incidence angle. Furthermore, it allows using the same grid topology around the wing for all configurations. The computational grid for the model in a free air environment contains 14.5 million cells.

Including the test section walls, the grid contains 20 million cells. The decomposition of the flow domain is based on 688 blocks for the wind tunnel test section with closed slots and 714 blocks for the wind tunnel with open slots. An example of the surface grid around the wing is presented in Fig. 4.

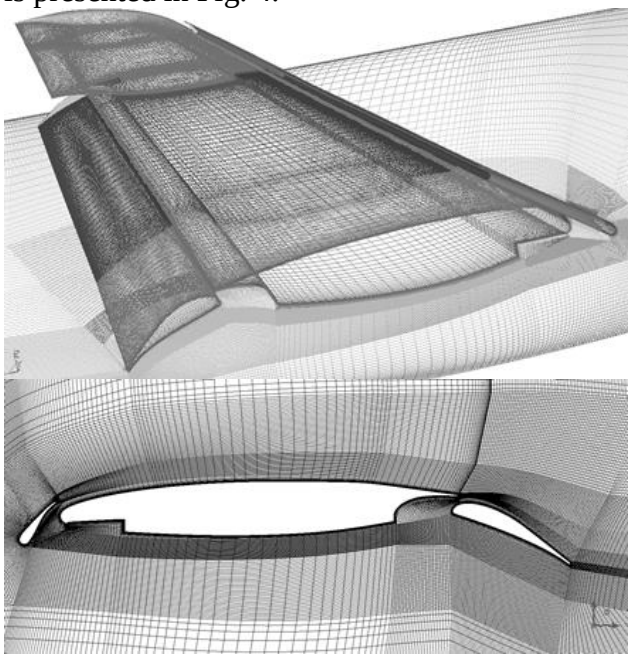

Fig. 4. Surface and cross section grid for the reference configuration

The number of cells along the wing span is 170, around the slat profile - 120, around the central section of wing – 250 and around the flap – 150. The boundary layer contains 33 cells. The distance from model to the boundaries of computational domain is approximately 4 m.

5 Numerical Results and Experimental Data Comparison

At the first stage of investigations the pressure distributions on wind tunnel walls were compared with experimental data. It holds important information because it gives a hint regarding walls interference corrections. Test results were obtained in a variety of regimes but with closed slots only. Appropriate calculations were performed for a similar geometry. Results of a comparison for the left side wall (facing the upper wing) at M=0.2, α = 18 deg are presented in Fig. 5.

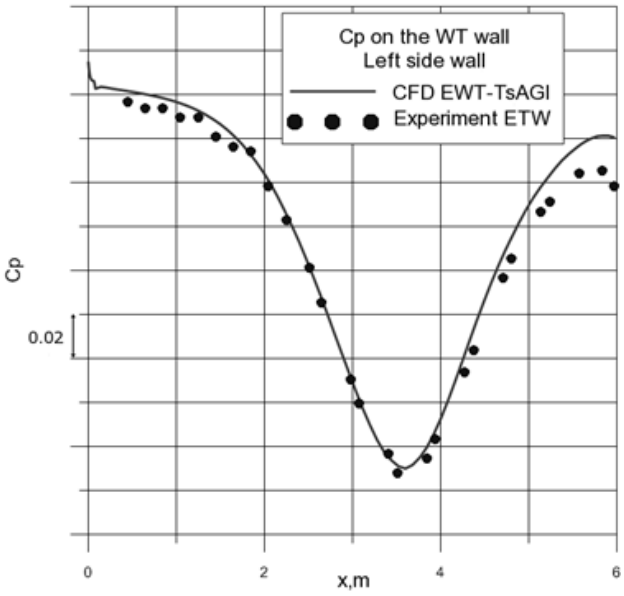

Fig. 5. ETW left side wall pressure distribution (facing upper wing)

The pressure distribution is dominated by the pressure drop generated by the flow acceleration on the upper side of the wing. The match of CFD data in this area is quite good as the maximal deviation is estimated to 1%. Increased deviations are to be seen towards the end of test section (x>5), where the influence of the re-entry might not yet be correctly calculated. Relevant considerations of the situation in this area are under investigation.

The pressure coefficients along wing chord are plotted for different span-wise cross sections in Fig. 6. The first section is at 16% span, located at an inboard part of wing. The last one is at 83% corresponding to the near tip section. Slat, main wing and flap can easily be distinguished. The pressure distribution along the slat upper surface (Krueger) shows an overshoot for CFD in the suction peak in comparison with the experimental data. On the lower surface there is a good agreement with experimental data to be stated indicating a mismatch of less than of 1% only. For the main wing, the obtained CFD solution is still in a better agreement with the experimental data for both wing sides. Differences appear with different signs (positive or negative) in comparison with the experiment. The lower surface is matching better than the upper one. This statement is also valid for the flap, where maximum differences up to 10% have been assessed.

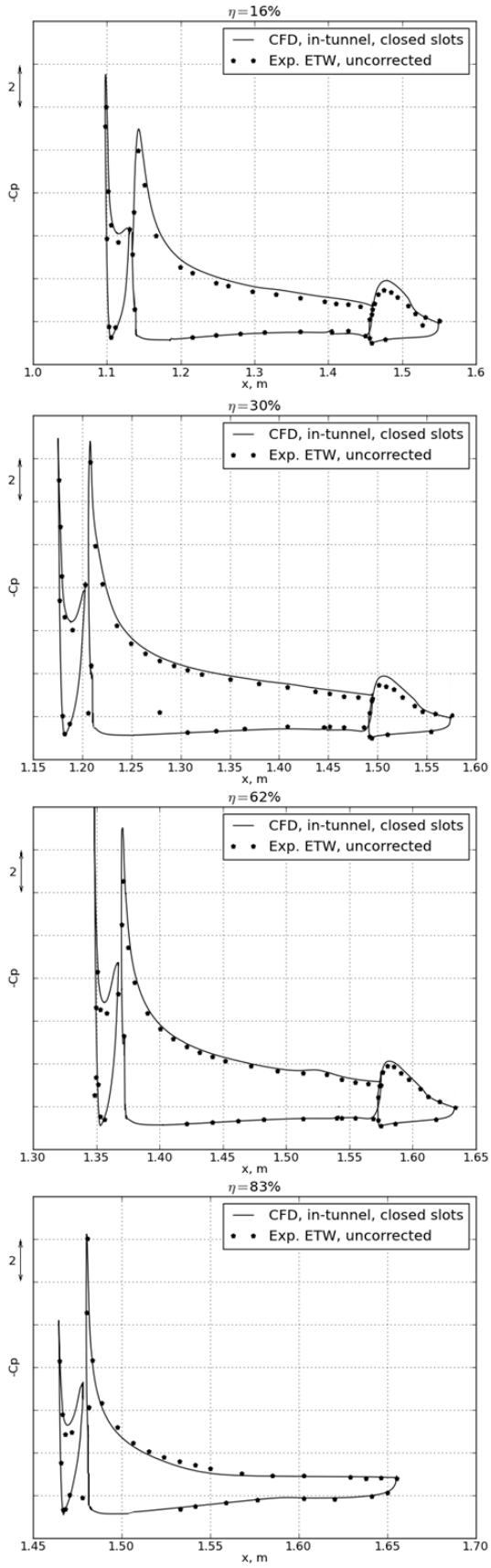

Fig. 6. Comparison of measured and calculated chord-wise pressure distributions at different span-wise positions

6 Influence of Wind Tunnel Walls on Stall calculated by CFD

Using slotted wall test section configurations for testing models at transonic speeds is one realized option for wind tunnels. In opposite, nearly all worldwide low speed facilities operate with close or open test sections. ETW holds the capability for running with closed or open side-walls when testing half-models at any speed. Referring to the classical wall interference assessment methods, no clear recommendation for closed or slotted can be given up to now. Here, the TsAGI Electronic Wind Tunnel offers a unique chance for tackling this problem. As a result, integral model performance in form of aerodynamic coefficients versus model incidence is given in Fig. 7-8.

For the considered landing configuration, CFD and experimental data are both acquired for wind tunnel conditions and presented without any corrections on to free flight conditions. The selected Mach number is equal to M=0.2; the Reynolds number is equal to 16.4 million. The computational grid for simulating the model inside the wind tunnel test section contains 20 million cells.

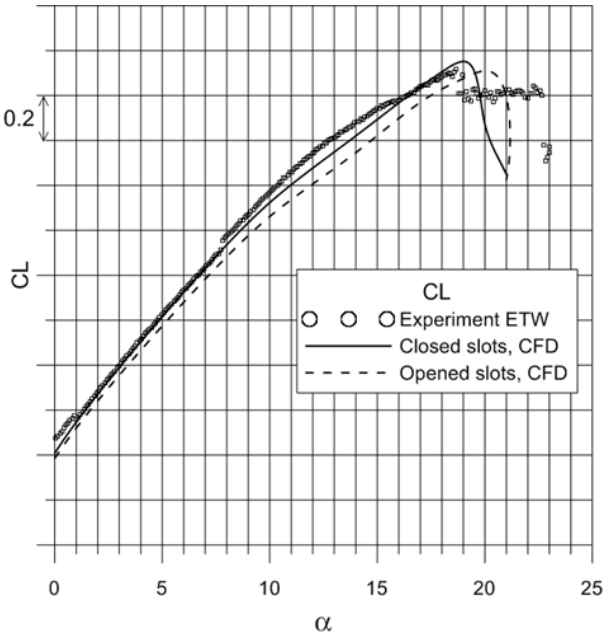

Fig. 7. Comparison of lift polars: CFD corresponds to ETW with open and closed slots; experiments in ETW were made with closed slots

The comparison of experimental and computational data of CL for the model installed in wind tunnel with closed walls demonstrates a good quality of CFD predictions. It is proven that the presence of wind tunnel walls leads to a growth of lift due to the contraction and acceleration of flow above the wing and due to deceleration from below, in the case of positive incidence angles. Consequently, closing the slots intensifies this effect. On the contrary, under stall conditions the influence of walls results in a reduction of lift. In this critical regime an additional contraction of flow will cause a decrease of the stall angle. For the model tested and investigated here, stall angle calculated by CFD would be reduced by about 1 deg, when comparing the wind tunnel with open slots with the closed slot configuration.

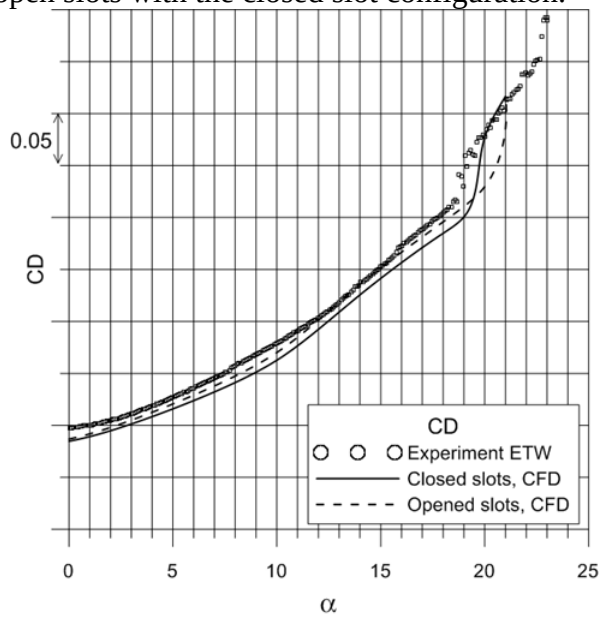

Fig. 8. Comparison of drag polars: CFD corresponds to ETW with open and closed slots; experiments in ETW were made with closed slots

References

[1] Neyland V.Ya., Bosnyakov S.M., Glazkov S.A., Ivanov A.I., Matyash S.V., Mikhailov S.V. and Vlasenko V.V. Conception of electronic wind tunnel and first results of its implementation. *Progress in Aerspace Sciences*, Vol. 37, No. 2, pp 121-145, 2001.

[2] Bosnyakov S.M., Akinfiev V.O., Vlasenko V.V., Glazkov S.A., Gorbushin A.R., Kazhan E.V., Kursakov I.A., Lysenkov A.V., Matyash S.V. and Mikhailov S.V. The Use of Computational Fluid Dynamics in TsAGI Experimental Works. *Mathematical Models and Computer Simulations*, Vol. 4, No. 3, pp 297-320, 2012.

[3] Piomelli U. Simulation: Achievements and Challenges. *Progress in Aerospace Sciences*, Vol. 35, pp 335–362, 1999.

[4] Wilcox D.C. *Turbulence Modeling for CFD*. 2nd edition, DCW Industries, 1998.

[5] Wilcox D.C. Reassessment of the Scale Determining Function for Advanced Turbulence Models. *AIAA Paper*, Vol. 19, No. 2, pp 1299–1310, 1988.

[6] Jones W.P. and Launder B.E. The Prediction of Laminarization with a Two Equation Model of Turbulence. *International Journal of Heat and Mass Transfer*, Vol. 15, pp 301–314, 1972.

[7] Launder B.E. and Sharma B.I. Application of the Energy Dissipation Model of the Turbulence to the Calculation of Flow near a Spinning Disc. *Letters in Heat and Mass Transfer*, Vol. 1, pp 131–138, 1974.

[8] Lam C.K.G. and Bremhorst K.A. Modified Form of the Model Predicting Wall Turbulence. *J. Fluids Eng.*, Vol. 103, pp 456–460, 1981.

[9] Menter F.R. Improved TwoEquation Turbulence Models for Aerodynamic Flows. *NASA TM103975*, 1992.

[10] Menter F.R., Langtry R.B., Likki S.R., Suzen Y.B., Huang P.G. and Völker S. A Correlation Based Transition Model Using Local Variables Part 1, Part 2 – Model Formulation. *SME-GT 2004-53452, ASME-GT2004-53454 ASME TURBO EXPO (Vienna, Austria)*, 2004.

[11] Jacobsen R.T. *The thermodynamic properties of nitrogen from 65 to 2000K with pressure to 1000atm*. Ph.D. thesis. Washington State University. NASA CR-128526, 1972.

[12] Quest J. High Quality Test Performance in Cryogenic Environment. *21st AIAA Aerodynamic Measurement Technology and Ground Testing Conf. AIAA 2000-2206, June 2000, Denver, CO, USA*.

[13] Quest J., Rolston S. and Wright M.C. ETW Investigation of a Modern Transport Aircraft Configuration over a Large Range of Reynolds Numbers. *40th AIAA Aerospace Sciences Meeting*, AIAA 2002-0422, January 2002, Reno, Nev. US.

Copyright Statement